

Multi-frequency atomic force microscopy: A system-theoretic approach

Naveen Shamsudhin ^{*,**} Hugo Rothuizen ^{**}
Bradley J. Nelson ^{*} Abu Sebastian ^{**}

^{*} *Institute of Robotics and Intelligent Systems, ETH Zurich,
8092 Zurich, Switzerland (e-mail: snaveen@ethz.ch)*

^{**} *IBM Research-Zurich, 8803 Rueschlikon, Switzerland*

Abstract: Multi-frequency atomic force microscopy (MF-AFM), employing the detection and/or excitation of multiple cantilever frequencies, has shown great promise in increasing the compositional sensitivity, and the spatial and temporal resolution of imaging. The multitude of frequency components generated in MF-AFM encode information about the tip-sample nonlinearity. For quantitative interpretation of the observables in MF-AFM operation, we propose a two-pronged approach combining special-purpose cantilevers and a system-theoretic modeling paradigm. This provides an excellent framework to understand and leverage the nonlinear dynamics of the interaction of a multi-eigenmodal cantilever with the nonlinear force potentials on the sample surface, to develop novel imaging methods. We describe experimental techniques for accurate in-situ identification of the cantilever (sensor/actuator) transfer functions, which are crucial components to understand the generation of MF-AFM observables. The modeling framework is verified with experiments and is shown to be able to predict several key features of MF-AFM operation.

Keywords: Atomic Force microscopy, MF-AFM, system identification, cantilever dynamics

1. INTRODUCTION

Since its invention in 1986 [Binnig et al. (1986)], the atomic force microscope (AFM) has been one of the quintessential instruments of nanoscale science and engineering. The tip-sample interaction force is sensed by a micro-cantilever and through this observation local surface properties are mapped with sub-nanometer resolution.

In the most basic form of AFM, the cantilever tip is scanned across the sample surface. Due to tip-sample interaction forces, the cantilever deflects and this deflection is measured. This is known as contact mode AFM. Given that the tip traverses over a short region of the tip-sample interaction potential, a linear analysis is usually sufficient to analyze this mode of AFM in spite of the highly nonlinear nature of the interaction force. However, contact-mode AFM has several drawbacks such as tip and sample damage owing to the lateral shear forces.

The next significant step in AFM was the introduction of dynamic mode operation [Martin et al. (1987)]. In this mode, the micro-cantilever is typically oscillated at the first resonance frequency to intermittently probe the sample. There are two key variants of dynamic-mode AFM. In amplitude modulation (AM-AFM) operation, the observables are the shift in the amplitude and phase of the cantilever oscillation. In frequency modulation (FM-AFM) operation, the cantilever is made to oscillate at the effective resonance frequency of the cantilever-sample system and the resulting frequency shift is the observable. Dynamic mode AFM is now an established tool for nanoscale investigation. The dynamics is much more involved given

that the tip traverses a wide range of the interaction potential. Hence, it took almost 20 years to fully establish the fundamental theory behind dynamic mode operation [Garcia and Herruzo (2012)].

In the last few years, there is a significant research effort towards multi-frequency AFM (MF-AFM). MF-AFM involves techniques where the cantilever motion is measured (and sometimes driven) at multiple resonant frequencies [Proksch (2011); Garcia and Herruzo (2012)]. These frequencies are usually associated with either the higher harmonics of the oscillation or the eigenmodes of the cantilever. MF-AFM provides several new information channels owing to the plethora of spectral components created, many of which can be mapped back into local surface properties. MF-AFM holds great promise in its ability to significantly enhance the resolution, the imaging throughput and the ability to discern material properties. The “holy grail” quest of AFM has been compositional mapping where materials differences are mapped out with the same nanometer resolution as topographic images. At present the most promising approach to reaching this goal is MF-AFM. However, in spite of the tremendous promise of MF-AFM techniques, quantitative MF-AFM remains a significant challenge. Interpreting and controlling the complex dynamics of the multi-modal cantilever interacting with the highly nonlinear and dissipative tip-sample interaction potential is an enormous challenge.

For quantitative MF-AFM, we need to utilize the full power of the theory of dynamical systems. Note that the MF-AFM dynamics is substantially more complicated than the regular dynamic mode AFM. The system-

theoretic approach to modelling AFM dynamics was first introduced for the analysis of AM-AFM dynamics [Sebastian et al. (2001), Sebastian et al. (2007)]. The systems viewpoint was also utilized in an elegant manner to obtain time-resolved tip-sample interaction forces [Stark et al. (2002)]. In this paper we extend this powerful modelling approach to investigate MF-AFM operation. We also propose accurate techniques to experimentally identify these multi-modal cantilever dynamics, correcting for the observation problem that arises from the commonly used optical beam deflection method. Using the systems model, we demonstrate an algorithm to recover the instantaneous tip-sample forces under any generic multi-tone cantilever excitation encompassing all common methods of MF-AFM operation, not limited to bi-modal, n-modal, inter-modal or band-excitation. We demonstrate the validity of the MF-AFM model through experiments using a tunable electrostatic force potential.

2. MICRO-CANTILEVERS FOR MF-AFM

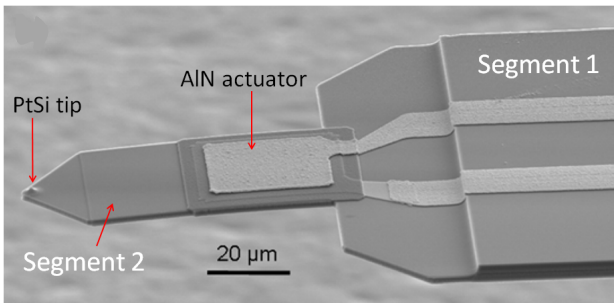


Fig. 1. Scanning electron micrograph of the fabricated MF-AFM cantilever. The cantilever possesses a stepped rectangular geometry with two segments.

The micro-cantilever is the transducer through which we probe tip-sample interaction forces. In contact-mode AFM, the only cantilever parameter of interest is its static stiffness. In traditional dynamic mode AFM, the parameters of interest are limited to the cantilever stiffness, resonant frequency and quality factor associated with the first eigenmode. Hence the dynamic response of the micro-cantilever over a wide frequency range was not of great interest. Moreover, these cantilevers are generally actuated by electrically exciting an externally mounted piezo-electric actuator. Spurious vibrational modes are introduced by the imperfect coupling between the external actuator and the micro-cantilever. Since the cantilevers are typically actuated and sensed at the first resonance frequency, these spurious modes did not pose much of a problem in traditional dynamic-mode AFM. However, for quantitative MF-AFM, it is essential to have a well-defined dynamic behaviour for the actuator-cantilever system. This could be achieved by integrating piezo-electric actuators onto the cantilever. In conventional rectangular cantilevers, there is a wide separation between the resonant frequencies corresponding to the different eigenmodes. For MF-AFM it is probably advantageous to reduce the spacing between the resonant frequencies to ensure significant coupling between the different modes.

Based on this, the authors recently introduced special MF-AFM cantilevers which have a stepped rectangular

geometry with two rectangular segments and integrated aluminum nitride actuators [Sebastian et al. (2012); Shamsudhin et al. (2012)]. They are also equipped with conductive platinum silicide tips [Bhaskaran et al. (2009)] for nanoscale electrical sensing. A scanning electron micrograph of one such cantilever is shown in Fig. 1. The new geometry spectrally close-packs the eigenmodes M_i , with the fourth eigenfrequency $\omega_{M_4} \approx 13.2 \cdot \omega_{M_1}$ compared to the rectangular case where $\omega_{M_4} \approx 34.4 \cdot \omega_{M_1}$. Furthermore, the integrated actuation allows for linear cantilever-actuator dynamics and an excellent phase response, making them well suited for quantitative MF-AFM.

3. MF-AFM MODELING FRAMEWORK

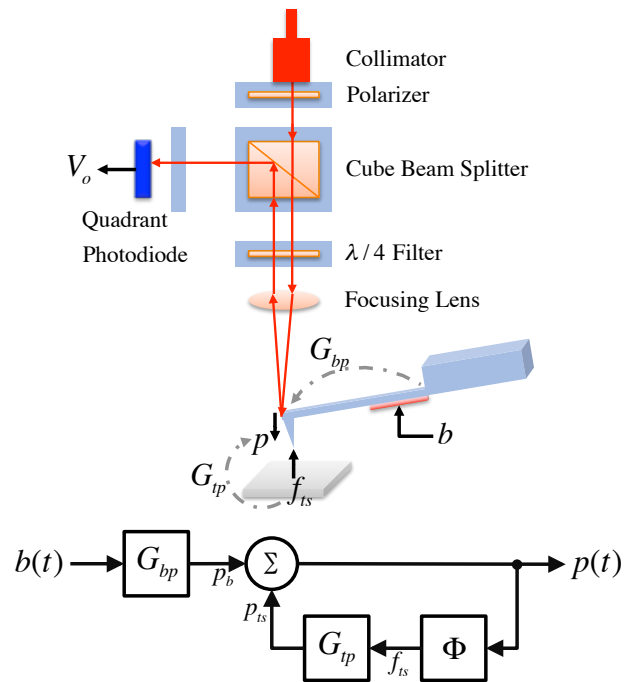


Fig. 2. Schematic illustration of the experimental setup and a system-theoretic model that captures the MF-AFM operation.

To interpret the complex dynamics of the above mentioned multi-modal cantilever interacting with a highly nonlinear tip-sample interaction force, we resort to a system-theoretic modeling framework, where the cantilever-sample interaction is modeled as the interaction between two distinct linear time-invariant cantilever models G_{bp} and G_{tp} interacting with the sample nonlinearity Φ (Fig. 2). The cantilever dynamics have been decoupled into two separate models, where the transfer function G_{bp} relates the tip displacement to the voltage signal applied to the piezo-electric actuator. This voltage signal is hitherto referred to as the base forcing signal, $b(t)$. G_{tp} relates the displacement to the force experienced by the tip. The tip-sample forces f_{ts} enter the feedback loop through G_{tp} , results in a displacement p_{ts} , which adds onto the displacement p_b generated by G_{bp} in response to $b(t)$. There is no restricting assumption on the nonlinearity Φ which may comprise of electric, magnetic or mechanical origin.

4. MODEL IDENTIFICATION

Next we present the in-situ experimental identification of the G_{bp} and G_{tp} transfer functions associated with the systems-model. A key challenge arises from the fact that optical beam deflection systems are widely employed to measure the cantilever deflection signal (see Fig. 2) necessitated by the requirements on bandwidth and resolution. However, the measured photodiode signal (V_o) is proportional to the relative angle generated at the end of the cantilever (i.e at the point of laser focus) and not to the absolute cantilever tip displacement [Marti (1999)].

It is common practice to identify the dynamics of the first eigenmode for regular dynamic mode AFM and only a few groups have tried to identify the multi-modal dynamics of the cantilever [Scherer et al. (2000), Stark et al. (2005), Pini et al. (2010)]. Multi-modal identification via thermal noise forcing is also demonstrated [Salapaka et al. (1997)], but it is not possible to obtain any useful phase information. But in all these approaches a methodology to identify the multi-modal displacement dynamics from the angular measurement is clearly lacking.

4.1 Base-Forcing Transfer Functions G_{ba} and G_{bp}

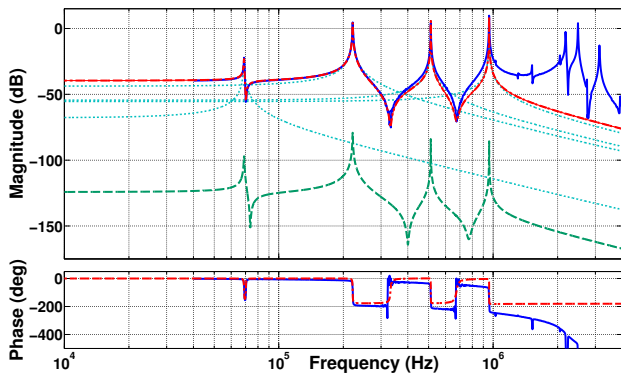


Fig. 3. Identification of base-forcing transfer functions; The measured angular response to a base excitation is shown in blue, the pole-zero fit G_{ba} in red, and the bi-quad expansion of the pole-zero model is shown in cyan, and finally G_{bp} is shown in green.

To identify the base-forcing transfer functions, the integrated actuator is driven with a single tone voltage signal, $b(t)$ and the input frequency is varied while simultaneously monitoring the photodiode signal, $V_o(t)$ using a lock-in amplifier. To obtain the angular information, $a(t)$ from the photodiode signal, V_o , it needs to be scaled by the inverse of a constant parameter, K_E . K_E is defined as $K_E = \alpha_0 \cdot D^{-1}$ where α_0 [rad/meter] is the ratio of the tip angle to the tip displacement generated by a static tip forcing and D [volts/meter] is the displacement sensitivity obtained from a standard approach curve. For a diving board cantilever, $\alpha_0 = (3/2) \cdot L$, where L is the cantilever length, but since ours has a dual-beam structure with integrated actuators and electrodes, we used finite-element analysis to estimate the ratio α_0 . The complete frequency response is recorded upto 2 MHz (Fig. 3). The drive signal is chosen to have a fixed peak-to-peak amplitude of 300 mV to ensure adequate signal-to-noise ratio and at the same time preserving the linearity of cantilever motion.

The resulting angular frequency response is fit with a pole-zero model (curve in red in Fig. 3) to the obtain G_{ba} (curve in blue in Fig. 3). The excellent fit further confirming the linearity of the frequency response. Remarkably the phase response shows a collocated dynamic behavior over a Megahertz bandwidth. We restrict our identification to the first four eigenmodes of the cantilever. Performing a biquad expansion on G_{ba} , we can rewrite it as a summation, which essentially represents an orthogonal summation of the first four eigenmodes of the cantilever.

$$G_{ba}(s) = \sum_{i=1}^4 \frac{\beta_i \omega_i^2}{s^2 + 2\zeta_{bi}\omega_i s + \omega_i^2} = \sum_{i=1}^4 H_{b,i}(s) \quad (1)$$

Now, to obtain G_{bp} (curve in green Fig. 3), we scale each of the eigenmodes $H_{b,i}$ by modal correction factors α_i ,

$$G_{bp}(s) = \sum_{i=1}^4 \left(\frac{1}{\alpha_i} \right) H_{b,i}(s) \quad (2)$$

α_i captures the angle generated by a unit displacement at the i th eigenmode and are obtained from finite element analysis. Thus we have identified both the transfer functions G_{ba} and G_{bp} .

4.2 Tip-Forcing Transfer Functions G_{ta} and G_{tp}

To identify the tip-forcing transfer functions, we need a mechanism to ensure forcing at the cantilever tip and to excite its multiple eigenmodes. We propose an identification strategy utilizing electrostatic tip forcing. The cantilever is made of n-doped silicon, this means that it can form a conductive plate of a capacitor. To create a confined electrostatic-forcing at a narrow region around the tip, we microfabricated pillars of dimensions $50 \mu\text{m}$ in height and $8 \mu\text{m}$ in diameter (see Fig. 4). There pillars were created on an n-doped silicon wafer using deep reactive ion etching process. The cantilever tip was then positioned approximately 200 nm above one of these pillars.

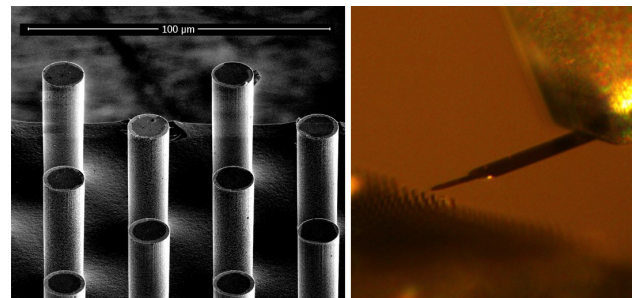


Fig. 4. Si pillars fabricated by DRIE positioned at the tip of the micro-cantilever. Scale bar: $100\mu\text{m}$

The net electrostatic force acting on the cantilever for a given pillar bias voltage V_e can be decomposed into the sum of three forces, essentially the tip-apex force, the tip-cone force, and the body force as proposed by Colchero et al. (2001).

$$f_{ts} = \Phi_e(V_e, p) = \Phi_{apex} + \Phi_{cone} + \Phi_{body} \quad (3)$$

Due to the confinement of the electrostatic field to a narrow region of tip, and for small cantilever deflections, we

can estimate a frequency-independent Φ_e linearly dependent on the square of the electrostatic voltage, $f_{ts} \approx A_0 \cdot V_e^2$

The silicon pillar was biased with a band-limited noise signal and the resultant photodiode signal, V_o was recorded at a sampling frequency of 10 MHz and the frequency response was estimated using Welch's averaged periodogram method. The linearity of the output response to the input electrostatic forcing is verified by the high coherence value of the identified frequency response and further confirmed by the excellent pole-zero fit as shown in Fig. 5. Following a similar calibration procedure as for identifying the base excitation dynamics G_{bp} , we scale each harmonic oscillator with the corresponding modal correction factors α_i .

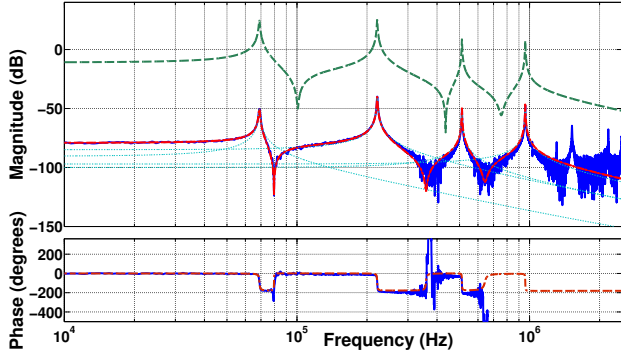


Fig. 5. Identification of tip-forcing transfer functions; The measured angular response to a tip excitation is shown in blue, the pole-zero fit G_{ta} in red, and the bi-quad expansion of the pole-zero model is shown in cyan, and G_{tp0} is shown in green.

$$G_{tp0}(s) = \sum_{i=1}^4 \left(\frac{1}{\alpha_i} \right) \frac{\gamma_i \omega_i^2}{s^2 + 2\zeta_{ti} \omega_i s + \omega_i^2} \quad (4)$$

The dc gain of the tip-forcing transfer function G_{tp} must equal the inverse of the cantilever static stiffness k_s . The static stiffness is typically determined by using the cantilever's thermal noise response or by *Sader's* method. Since both techniques use theoretical calibration factors based on rectangular cantilever geometries, we employ a calibrated *FemtoTools* MEMS force sensor to directly quantify the stiffness of the cantilever. The force sensor is used to measure the restoration force when the cantilever tip is pressed against it.

Finally the transfer function, G_{tp} is obtained as,

$$G_{tp}(s) = \frac{1}{k_s} \frac{G_{tp0}(s)}{|G_{tp0}(j0)|} = \sum_{i=1}^4 H_{tp,i} \quad (5)$$

4.3 Optical Filter S_b and S_t

From the identified transfer functions G_{ba} , G_{bp} , G_{ta} , G_{tp} , we can derive two filters S_b and S_t given by

$$S_b(\omega_n) = \left| \frac{G_{ba}}{G_{bp}} \right| \text{ and } S_t(\omega_n) = \left| \frac{G_{ta}}{G_{tp}} \right| \quad (6)$$

and the magnitude response of the filters is shown in Fig. 6.

These zero-phase filters capture the effect of the optical beam deflection system, namely the translation from tip

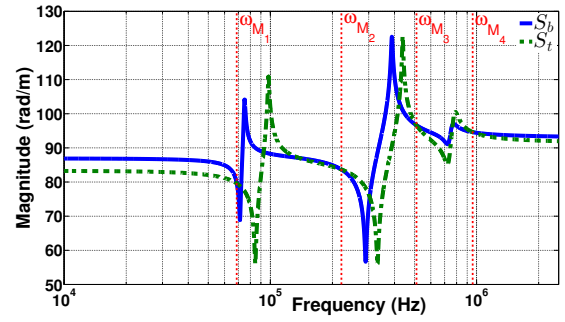


Fig. 6. Magnitude response of the optical filters S_b and S_t .

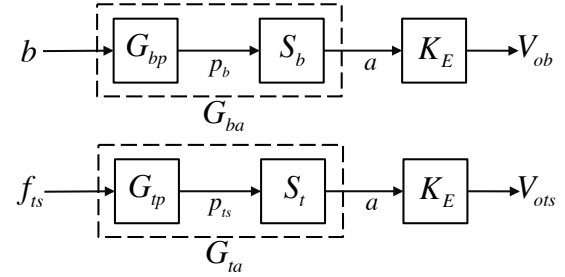


Fig. 7. Block diagram description of the measurable photodiode signal and the forcing signals.

displacement signal to the angular signal. For example, the measurable photodiode signal arising from forcing the cantilever with a base forcing signal, $b(t)$ or a tip forcing signal, $f_{ts}(t)$ is schematically shown in Fig. 7. These filters are essential in de-convolving the tip displacement from the measured photodiode signal during MF-AFM operation as illustrated in the next section.

5. SIGNAL FLOW IN MF-AFM

Based on the identified G_{bp} , G_{tp} , K_E and the optical filters S_b and S_t , we can now create an accurate description of the tip displacement as well as the tip-sample interaction forces.

5.1 Tip Displacement in MF-AFM

If the cantilever is actuated with an M -tone base forcing signal $b(t)$, in the absence of tip-sample interaction forces, the linearity of G_{bp} ensures that the tip response $p_b(t)$ is also M -toned given by,

$$p_b(t) = \sum_{\omega=1}^M p_f(\omega) = G_{bp} \left\{ \sum_{\omega=1}^M b(\omega) \right\} \quad (7)$$

$$\text{where } \omega = [\omega_1, \dots, \omega_{M_1}, \dots, \omega_M] \in \mathbb{R}^M$$

However, in the presence of a sample nonlinearity, Φ , the interaction of the M -tone driven-cantilever with Φ generates spectral components in the tip motion which are different from the actuation frequencies, including harmonics and intermodulation products. The net displacement of the cantilever tip $p(t)$ can be written as the summation of the displacements $p_b(t)$ and $p_t(t)$ induced by the base forcing and the tip forcing from the sample respectively (Fig. 2).

$$p(t) = G_{bp} b(t) + G_{tp} f_{ts}(t) \quad (8)$$

$$p(t) = p_b(t) + p_{ts}(t) \quad (9)$$

The corresponding photodiode signal can also be written as a summation,

$$V_o(t) = V_{ob}(t) + V_{ots}(t) \quad (10)$$

By taking the discrete fourier transform DFT of the sampled photodiode signal, we can express Eq. (10) as

$$V_o(\omega_n) = \sum_{i=0}^{N-1} V_o(t_i) e^{-j2\pi i n/N} \quad (11)$$

$$V_o(\omega_n) = V_{ob}(\omega_n) + V_{ots}(\omega_n) \quad (12)$$

The contribution of the tip-forcing displacement p_{ts} coming from the sample can be estimated by removing the base actuation component from the measured photodiode signal V_o .

$$V_{ots}(\omega_n) = V_o(\omega_n) - K_E \cdot S_b(\omega_n) \cdot p_b(\omega_n) \quad (13)$$

$$p_{ts}(\omega_n) = \frac{1}{K_E} \cdot S_t^{-1} \cdot V_{ots}(\omega_n) \quad (14)$$

Taking the inverse DFT of Eq (14), we arrive at the displacement p_{ts} generated by the tip-sample forces f_{ts} ,

$$p_{ts}(t_i) = \frac{1}{N} \sum_{n=0}^{N-1} p_{ts}(\omega_n) e^{j2\pi i n/N} \quad (15)$$

One of the perennial challenges of AFM is the accurate description of the instantaneous tip-sample interaction forces. Using the experimentally identified model components along with the system-theoretic framework, the tip-sample forces f_{ts} in MF-AFM experiments can be directly estimated without any prior assumptions of the parametrization of the forcing nonlinearity Φ . We can reformulate Eq.(8), and solve for the tip-sample force as follows,

$$f_{ts}(t) = G_{tp}^{-1} \{p(t) - G_{bp} b(t)\} \quad (16)$$

5.2 Experimental demonstration

To verify the systems-model in a multi-frequency AFM scenario, electrostatic forcing was again chosen as the candidate for generating the tip forcing signal. A block diagram representation is shown in Figure 8. The electrostatic forcing operator, denoted by Φ_e will generate a force that is a function of the voltage signal, V_e and the tip displacement, $p(t)$.

An experiment is performed whereby the cantilever tip is positioned above the Si pillar (as shown in Fig. 4). The cantilever is actuated bi-modally at its first two eigenfrequencies with $b(t) = 0.6 \sin(\omega_{M_1} t) + 0.05 \sin(\omega_{M_2} t)$. Based on the systems-model, by suitable selection of $V_e(t)$, each of the eigenmodal vibrations are cancelled selectively

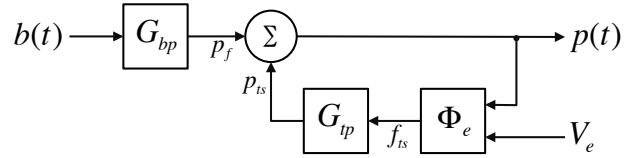


Fig. 8. Systems-model for electrostatic cantilever forcing.

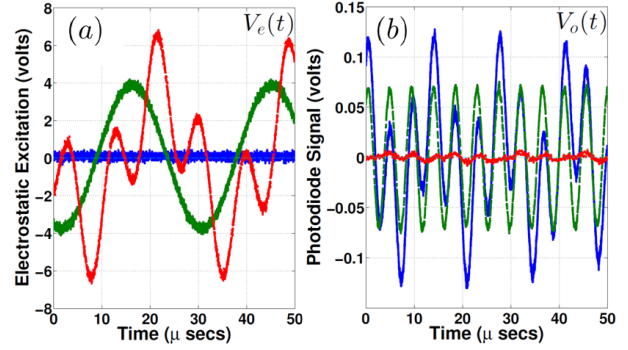


Fig. 9. Experimental validation of the systems-model (a) Electrostatic forcing signal $V_e(t)$ (b) Corresponding photodiode deflection signal $V_o(t)$; No cancellation in blue, eigenmode M_1 cancellation in green, and bi-modal (M_1 and M_2) cancellation in red.

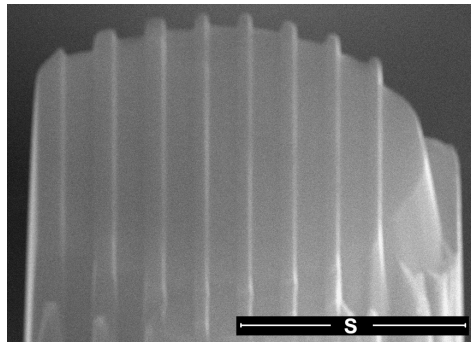
as shown in Fig. 9. Fig. 9(b) shows the photodiode signal whereas 9(a) shows the corresponding $V_e(t)$ signal. This is a strong validation of not just the systems-model, but also of the various steps involved in the model identification process.

Next we present imaging experiments where the cantilever tip was scanned in non-contact mode above the surface of the Si pillar which had been milled by a focused ion beam (FIB) to produce narrow stripes (see Fig. 10(a)). As the cantilever tip is scanned above this sample, the topography variation of the stripes creates a varying Φ_e consequently modulating the force f_{ts} felt by the tip.

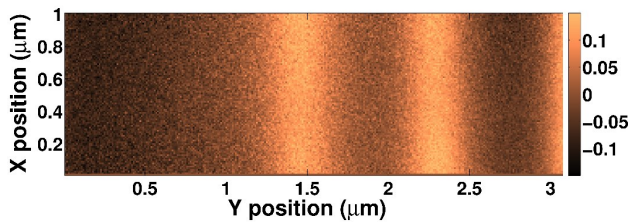
In the first experiment, the pillar was biased with a voltage signal at half the second eigenmodal frequency $V_e(t) = V_{e0} \sin(2\pi \frac{\omega_{M_2}}{2} t)$ while $b(t) = 0$. Fig. 10(b) shows the demodulated ω_{M_2} amplitude. In this scenario, the resulting amplitude signal is enhanced due to the forcing at the tip apex caused by the protruding stripes, while the background signal from cantilever body is low. In the second experiment, we additionally apply a base excitation $b(t) = \sin(2\pi \omega_{M_2} t + \phi)$ which in accordance with the systems-model should cancel the M_2 oscillation when the cantilever is above the stripes. The resulting image is shown in Fig. 10(c) where this cancellation is clearly visible. This experiment serves as a further validation of the modeling approach as well as provides insight into development of directed MF-AFM operation modes in the future.

6. CONCLUSIONS

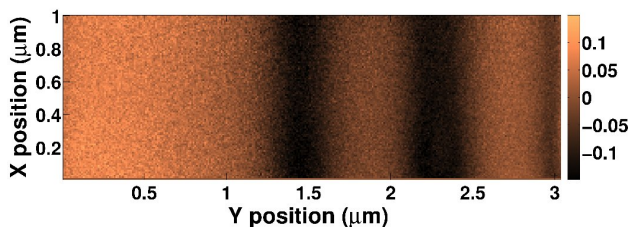
Quantitative multi-frequency AFM is a challenging problem where system-theoretic approaches can play a significant role especially in combination with experimental tools such as micro-cantilevers with well defined dynamic behaviour over MHz bandwidth. In this article we illustrate



(a) Scale Bar $S = 4\mu\text{m}$



(b) $V_e(t) = V_{e0}\sin\left(2\pi\frac{\omega_{M_2}}{2}t\right)$ and $b(t) = 0$



(c) $V_e(t) = V_{e0}\sin\left(2\pi\frac{\omega_{M_2}}{2}t\right)$ and $b(t) = \sin\left(2\pi\omega_{M_2}t + \phi\right)$

Fig. 10. (a) Scanning electron micrograph of the structures created using the FIB. (b,c) Images obtained based on the ω_{M_2} amplitude signal.

this by unravelling the complex dynamics arising from such a cantilever interacting with nonlinear tip-sample interaction forces using a systems-model. The various elements of the model are experimentally identified. In particular, an experimental methodology is proposed to overcome the challenge posed by optical beam deflection systems that are used to sense the cantilever deflection signal. Accurate description of the tip displacement as well as the instantaneous tip-sample interaction force is derived from the observable photodiode signal. Finally, experimental results are presented to validate the modeling framework where the tip-sample interaction forces are generated through electro-static means.

ACKNOWLEDGEMENTS

We would like to thank M. Despont for contributions to the cantilever design and P. Jonnalagadda for clean-room support. We thank the Swiss National Foundation for their financial support through the SystemsX.ch project MecanX.

REFERENCES

Bhaskaran, H., Sebastian, A., and Despont, M. (2009). Nanoscale pti tips for conducting probe technologies. *Nanotechnology, IEEE Transactions on*, 8(1), 128–131.

- Binnig, G., Quate, C.F., and Gerber, C. (1986). Atomic force microscope. *Physical review letters*, 56(9), 930.
- Colchero, J., Gil, A., and Baró, A. (2001). Resolution enhancement and improved data interpretation in electrostatic force microscopy. *Physical Review B*, 64(24), 245403.
- Garcia, R. and Herruzo, E.T. (2012). The emergence of multifrequency force microscopy. *Nature nanotechnology*, 7(4), 217–226.
- Marti, O. (1999). *Handbook of Micro/Nanotribology*, chapter AFM Instrumentation and Tips, 81–144. CRC Press, 2nd edition.
- Martin, Y., Williams, C.C., and Wickramasinghe, H.K. (1987). Atomic force microscope–force mapping and profiling on a sub 100-Å scale. *Journal of Applied Physics*, 61(10), 4723–4729.
- Pini, V., Tiribilli, B., Gambi, C.M.C., and Vassalli, M. (2010). Dynamical characterization of vibrating afm cantilevers forced by photothermal excitation. *Phys. Rev. B*, 81, 054302.
- Proksch, R. (2011). Multi-frequency atomic force microscopy. In *Scanning Probe Microscopy of Functional Materials*, 125–151. Springer.
- Salapaka, M., Bergh, H., Lai, J., Majumdar, A., and McFarland, E. (1997). Multi-mode noise analysis of cantilevers for scanning probe microscopy. *Journal of Applied Physics*, 81(6), 2480–2487.
- Scherer, M.P., Frank, G., and Gummer, A.W. (2000). Experimental determination of the mechanical impedance of atomic force microscopy cantilevers in fluids up to 70 khz. *Journal of Applied Physics*, 88(5), 2912–2920.
- Sebastian, A., Salapaka, M.V., Chen, D.J., and Cleveland, J.P. (2001). Harmonic and power balance tools for tapping-mode atomic force microscope. *Journal of Applied Physics*, 89(11), 6473–6480.
- Sebastian, A., Gannepalli, A., and Salapaka, M.V. (2007). A review of the systems approach to the analysis of dynamic-mode atomic force microscopy. *Control Systems Technology, IEEE Transactions on*, 15(5), 952–959.
- Sebastian, A., Shamsudhin, N., Rothuizen, H., Drechsler, U., Koelmans, W.W., Bhaskaran, H., Quenzer, H.J., Wagner, B., and Despont, M. (2012). Note: Micro-cantilevers with aln actuators and pti tips for multi-frequency atomic force microscopy. *Review of Scientific Instruments*, 83(9), 096107–096107.
- Shamsudhin, N., Rothuizen, H., Despont, M., Lygeros, J., and Sebastian, A. (2012). Micro-cantilever design and modeling framework for quantitative multi-frequency afm. In *Nanotechnology (IEEE-NANO), 2012 12th IEEE Conference on*, 1–5.
- Stark, M., Guckenberger, R., Stemmer, A., and Stark, R.W. (2005). Estimating the transfer function of the cantilever in atomic force microscopy: A system identification approach. *Journal of Applied Physics*, 98(11), 114904–114904–7.
- Stark, M., Stark, R.W., Heckl, W.M., and Guckenberger, R. (2002). Inverting dynamic force microscopy: From signals to time-resolved interaction forces. *Proceedings of the National Academy of Sciences*, 99(13), 8473–8478.